Materials Horizons

Machine Learning-Assisted X-ray Absorption Analysis of Bimetallic Catalysts

Journal:	*Materials Horizons*
Manuscript ID	MH-REV-03-2025-000387.R1
Article Type:	Review Article
Date Submitted by the Author:	11-May-2025
Complete List of Authors:	Xiang, Shuting; Stony Brook University, Knecht, Marc; University of Miami, Department of Chemistry Frenkel, Anatoly; Brookhaven National Laboratory, Chemistry

Bimetallic nanoparticles have many novel functionalities compared to the bulk metals and their monometallic counterparts. Several recent developments highlight the role of reactions on inducing restructuring of bimetallic components on the nanoparticle surfaces and the paucity of experimental methods capable of detecting the effects occurring on or near the surface. Machine learning methods have demonstrated strong potential for analysis and modeling of X-ray absorption spectra in a broad range of materials due to the sensitivity of the spectra to the catalyst structure. In this review, both the limitations of conventional XAS analysis and the recent development aimed at overcoming them based on the use of machine learning methods are discussed. Among the most important new capabilities that emerge are the determination of bimetallic motifs in multi-component systems with poor Z-contrast, such as high-entropy alloys.

No primary research results, software or code have been included and no new data were generated or analysed as part of this review.

MINIREVIEW

Machine Learning-Assisted X-ray Absorption Analysis of Bimetallic Catalysts

Received 00th January 20xx,
Accepted 00th January 20xx

DOI: 10.1039/x0xx00000x

Shuting Xiang,[a] Marc R Knecht [b] and Anatoly Frenkel [a,c*]

Bimetallic nanoparticles have attracted increasing scientific and technological interest as modules for creating nanoscale materials with unique magnetic, electronic, and chemical properties. The properties of bimetallic NPs are functions of composition, size, shape, stoichiometry, and possibly internal structure (alloy or core-shell-like). Bimetallic nanoparticles have superior properties for catalytic application. However, it is challenging to understand and control the size, shape, composition, and activity of these nanomaterials. The internal atomic structure of these materials needs to be precisely characterized to understand the structure-function relationship. X-ray absorption fine structure (XAFS) spectroscopy has been a premiere tool for analyzing the compositional and structural motifs in bimetallic nanoparticles for several decades. In this review, we discuss the limitations in the ability of XAFS to detect catalytically relevant surface species and focus on recent developments in machine learning-assisted XAFS analysis aimed at overcoming these limitations.

1. Introduction

Bimetallic nanoparticles (BNPs) are composed of two distinct metals, offering enhanced properties compared to their monometallic counterparts, which has drawn significant attention from both technological and scientific communities. The properties of BNPs are influenced by the compositional motifs of the constituent metals and their nanoscale size, non-bulklike shape, and/or structure, which results in unique optical, electronic, magnetic, thermal, and catalytic effects that differ from pure elemental particles or bulk alloys.[1-3] They can be incorporated into nanocomposites by supporting them on organic or inorganic materials, further improving their properties.[4-6] The reduced size and increased surface area of BNPs make them particularly effective as catalysts in various applications.[7-10] Extensive research has focused on engineering novel types of BNPs, with recent efforts aimed at selectively producing new types of alloys, core-shell structures, and contact aggregates.[11, 12]

Fundamental studies of the synthesis, catalysis, and structure of bimetallic catalysts have been a fast-growing and exciting field for energy conversion and chemical transformations, such as for the oxygen reduction reaction (ORR), hydrogenation, dehydrogenation, CO methanation, formic acid oxidation, CO oxidation, water-gas shift reaction, etc.[13-16] The catalytic performances, such as activity, selectivity, and stability can be tuned through flexible modification of electronic and/or structural factors by adding a second metal (the guest metal) to the first metal (the host metal).[14] Thus, bimetallic catalysts have the capability of improving catalytic activity, enhancing catalytic selectivity, increasing catalytic stability, and lowering the cost of catalysts by tuning the compositions of constituent metals. A variety of compositional motifs in BNPs offers another knob for tuning their functionality. They can be divided into three main groups: an alloy, intermetallic, or nanocomposite structure (Fig. 1). Alloy catalysts have different forms, ranging from the bulk, surface, and near-surface alloys.[11, 14] Nanocomposite structures include core-shell structured bimetallic nanoparticles, nano dendrites, and others. Due to the diversity of bimetallic catalysts, tuning catalytic performance of a host metal could be performed through (a) an ensemble or geometric effect in which the coordination of atoms of a guest metal to an atom of the host metal on the surface provides new geometries of active sites or (b) the electronic or ligand effect wherein the addition of a guest metal alters the electronic properties of the active sites of the host metal by changes in the electron density at the active site metal. It is important to notice that it is difficult to disentangle these effects because, in some cases, all effects occur simultaneously to affect the performance and stability of the BNPs.[17]

In most cases, the difference in catalytic performance between bimetallic catalysts can be rationalized through the details of their size, structure, and compositional details. Those characteristics are prone to change due to the restructuring of the catalysts during the reaction.[18] That, in turn, motivates the fundamental studies of bimetallic catalysts toward understanding them at the atomic level and in real-time during catalytic reactions in relevant conditions of

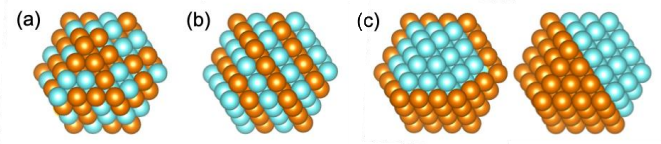

Fig. 1. Schematic of the three common groups of bimetallic structures: alloy (a), intermetallic (b), and two possible variations of nanocomposites (c).

[a] Materials Science and Chemical Engineering Department, Stony Brook University, Stony Brook, NY 11794, USA
[b] Department of Chemistry, University of Miami, Coral Gables, Florida 33146, USA
[c] Chemistry Division, Brookhaven National Laboratory, Upton, NY 11973, USA

temperature and pressure. Out of the limited number of methods applicable for this purpose, this review focuses on X-ray absorption fine structure (XAFS) spectroscopy, a powerful local structural probe that can interrogate not only the atomic-scale features of the BNPs in real reaction conditions but correlate them with the overall catalytic performance.

XAFS is typically divided into two regimes: X-ray absorption near edge structure (XANES) and extended X-ray absorption fine structure (EXAFS). XANES can be used to extract information about the oxidation state, three-dimensional geometry, and coordination environment of elements under investigation. EXAFS is used to determine the distances, coordination number (CN), and neighbour species of the absorbing atom. From the time EXAFS was recognized as a new structural tool (at the beginning of the 1970s),[19] its application to studies of BNPs was among the first of all materials characterization works using this technique.[20, 21] The use of EXAFS allowed researchers to obtain partial CNs, interatomic distances between different types of atoms and their structural and dynamic disorder factors, which can provide useful structural information for catalysis. For example, a strong correlation exists between the CN of atoms on the surface and the nanoparticle size and facet, which plays a critical role in heterogeneous catalysis.[22] In recent work, the Pd-Pd bonds in monomers, dimers, or trimers (Pd_1Au, Pd_2Au, or Pd_3Au) in dilute Pd-in-Au alloys was shown to directly affect their catalytic activity to hydrogen-deuterium exchange,[23] CO oxidation[24] and selective hydrogenation[25, 26] reactions.

While XAFS has been a workhorse technique for catalysis research, it was also recognized that it has several notable limitations. Chief among them are: 1) EXAFS oscillations can be difficult to detect with a good signal-to-noise ratio in the case of dilute concentrations of real catalysts, high temperatures, harsh reaction conditions, etc., and 2) EXAFS has limited sensitivity to the catalytic species at the nanoparticle surfaces as it is an ensemble-averaging technique. An example of dilute bimetallic alloys mentioned above can be used to illustrate these challenges. While the distribution of metal ensembles on the nanoparticle surface is of key interest, XAFS spectra of the surface ensembles are dwarfed by the bulk spectra of the same absorbing element, where separating the surface contributions from the bulk becomes very challenging. In addition, EXAFS is limited in its ability to determine the coordination of bimetallic components if they contain elements that are neighbours in the periodic table.

Recent applications of machine learning (ML) to the structural refinement of XAFS spectra have shown strong promise in addressing these challenges. ML techniques offer a powerful alternative to conventional tools for decoding the structural details "hidden" in the spectra. In this review, we focus on the overview of the progress made in the last decade toward the development of the ML-XANES and ML-EXAFS methods and their applications to solving these and other challenges for determining the structural and compositional motifs in BNPs. This review does not include such topics as enhancing XAFS analysis by combining it with other techniques, such as electron microscopy, X-ray photoelectron spectroscopy, infrared spectroscopy, and others,[7, 25, 27-30] as well as sensitivity-enhancing methods such as modulation excitation spectroscopy which are extensively covered elsewhere.[31-34]

Due to our larger focus on the functionality of the BNPs and the long-term goal of improving techniques for their rational design, we are adopting a "descriptor" approach to their characterization, searching for those attributes of structure and electronic properties that can be, on one hand, extracted from the experimental data, and, on the other hand, theoretically modelled. Therefore, we are focused on the "inverse" methods of structural analysis, where the starting point is the experimental data, and the endpoint is a list of generalized descriptors of the structure, dynamics, and electronic properties. Examples of such descriptors may include the coordination numbers of nearest neighbours, interatomic distances, surface strain, *d*-band center, and many others. The "forward" methods for the analysis of XANES spectra, including those assisted by ML (in this approach, the theoretical spectra are generated using different structural models and compared with the experiment), are the focus of intense research as well and are beyond the scope of this review.

2. Machine learning–assisted XAFS analysis on BNPs

In this section, we will introduce the main idea behind spectral inversion using an artificial neural network and demonstrate its application to XANES and EXAFS spectra. The main idea behind the original application of supervised ML to the XANES spectra of monometallic nanoparticles was to extract key structural characteristics, the pair CNs. These data can be used as indices of the size, shape, and morphology of the nanoparticles, but are difficult to measure by EXAFS due to the limitations described above. For BNPs, partial CNs were used to extract the compositional information as summarized above. In both cases, an artificial neural network was trained on a theoretical data set comprising hundreds of thousands of spectra generated using FEFF[35] and FDMNES[36] theoretical spectroscopy codes. By using both codes for the neural network training, some systematic errors present in them are partially compensated.[37]

2.1 Machine learning–assisted XANES analysis

For monometallic NPs, the training set (the labels were the CNs of several nearest neighbouring shells) was constructed using a combinatorial approach, in which the theoretical spectrum $\mu^i(E)$ was averaged over a sequence *i* of *n* randomly chosen, site-specific XANES calculations, and could be labelled by well-defined, site-average CNs:[38]

$$\mu^i(E) = \sum_{j=1}^{n} \mu_j(E)/n\,,$$
$$C_1{}^i = \sum_{j=1}^{n} c_{1j}/n,$$
$$C_2{}^i = \sum_{j=1}^{n} c_{2j}/n, \quad \ldots \qquad (1)$$

Here, c_{1j}, c_{2j}, … are the CNs of the first, second, etc., neighboring shells for sites *j* within the sequence *i*.

For bimetallic materials, the edge region of the XAS spectrum for each type of atomic species can be used to provide information on the first nearest neighbour pairs of four types: C_{AA}, C_{AB}, C_{BA}, and C_{BB}. Therefore, the method for obtaining the CNs from the XANES spectra relies on two independent, ''absorber-specific'', neural

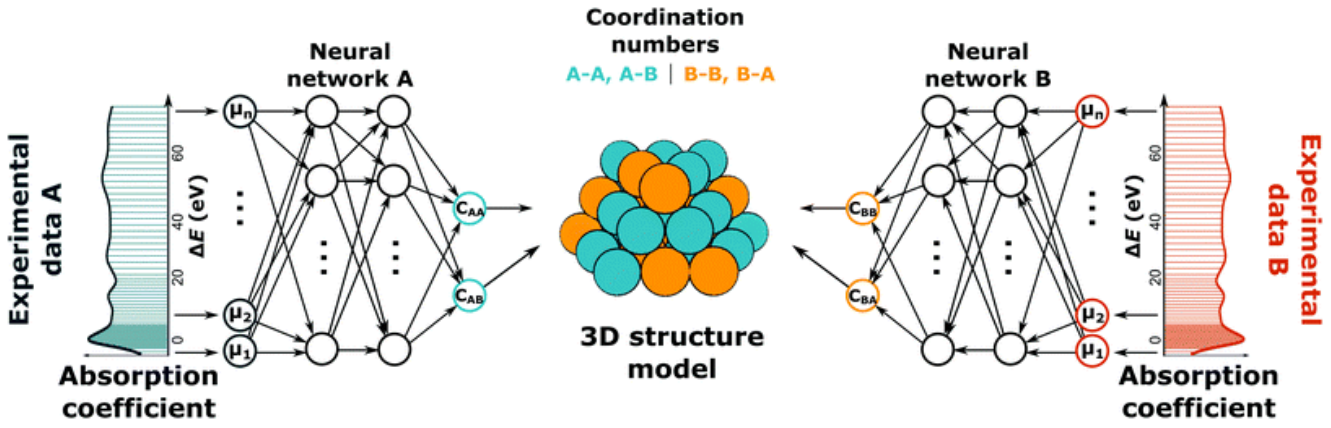

Fig. 2. A schematic that represents the application of NN-XANES to an A_xB_{1-x} bimetallic system. Partial first CNs are extracted from the XANES of A and B absorbing components. The partial CNs (A–A, A–B, B–B, and B–A) are used to deduce the average nanoparticle structure. Reproduced with permission from Ref. 38.

networks, each with ''pair-specific'' outputs (*i.e.*, C_{AA}, C_{AB} for absorber A, and C_{BA} and C_{BB} for absorber B - Fig. 2).[39] The training of each neural network (NN) was performed using a diverse, labelled set constructed using linear combination of the site-specific, theoretical XANES spectra (*i.e.*, similarly to the method in Eq. (1)):

$$\text{A edge: } \mu^i(E) = \sum_{j=1}^{n} \mu_j(E)/N_A,$$
$$C_{AA}{}^i = \sum_{j=1}^{n} c_{AAj}/N_A,$$
$$C_{AB}{}^i = \sum_{j=1}^{n} c_{ABj}/N_A, \quad (2)$$

$$\text{B edge: } \mu^i(E) = \sum_{j=1}^{n} \mu_j(E)/N_B,$$
$$C_{BA}{}^i = \sum_{j=1}^{n} c_{BAj}/N_B,$$
$$C_{BB}{}^i = \sum_{j=1}^{n} c_{BBj}/N_B. \quad (3)$$

Several methods were discussed in literature for minimizing the systematic errors of NN predictions due to the effects of experimental noise, differences between theoretical spectra and experimental data, overfitting, etc. One advantage of the NN-based approach to XANES analysis in dealing with systematic errors is the nonlinear nature of NN: during the training, NN assigns larger weights to those spectral features that are relatively more important for the determination of descriptors and hence can perform better than, e.g., linear methods in presence of systematic errors or experimental noise.[37] Timoshenko, Frenkel et al., found that the systematic errors of NN predictions can be reduced significantly if the difference in absorption coefficient between the NP spectrum and corresponding bulk spectrum of the same element were used for prediction, not the NP spectrum itself.[38] To estimate error bars, many groups study model performance after repeating training 5-10 times and applying the model to the same data and different values of hyperparameters and random seeds.[38, 40] Standard deviations in the predicted values due to this variability are commonly reported as error bars. Recently, a neural network ensemble (NNE) method was applied for quantifying the uncertainties of predicting XAS spectra on out-of-sample data.[41] Finally, transfer learning approaches have been used to improve the quality of the prediction based on theoretical training sets.[42]

2.2 Examples of the use of ML-XANES approach for structural characterization of BNP catalysts

Using the ML-XANES for BNPs opens an avenue for structural characterization and modelling of the materials based on their CNs, which was previously limited to EXAFS analysis only. In principle, the partial CNs (C_{AA}, C_{AB}, C_{BA}, C_{BB}) can be obtained in the entire range of compositions from ML-XANES analysis.[39, 43-46] That is an invaluable advantage over EXAFS in the case of dilute metal loading, harsh reaction conditions, and/or high structural disorder in the BNPs, in which EXAFS data may be of either very poor quality or unavailable (as in the case of the size-selective bimetallic clusters on a flat support[43]). There, ML-XANES stands out as the only tool that can be used for quantifying the neighbouring pairs, as demonstrated for Cu_3Pd and Cu_4Pd bimetallic clusters containing either four or five atoms, respectively.[43]

In the case when constituting elements are neighbours on the periodic table and thus have poor Z contrast, EXAFS modelling cannot be used to extract partial CNs from the data (although CNs corresponding to the A-M and B-M pairs, where M = A or B, can be still obtained in such cases[47, 48]). ML-XANES, on the other hand, has the sensitivity to these spectral features, and those are strongly affected by the CNs of different neighbouring types to the X-ray absorber due to the strong sensitivity to electronic charge transfer between the alloying atoms. In recent work, Frenkel, Knecht, and coworkers demonstrated the power of ML-XANES for analysing Pt-Au BNPs and determining their CNs for structural modeling.[44-46]

This approach combined ML-assisted refinement of XAFS was utilized for structural and compositional analyses.[44] In this study, the NN was constructed to build a correlation between the XANES spectra and the CNs of the first nearest neighbouring pairs Au–Au, Au–Pt, Pt–Au, and Pt–Pt. The validation results of the NN in Fig. 3 show that it can provide good predictions on the partial CNs from theoretical XANES spectra.[44]

BNPs, in which one species is dilute, have attracted significant interest for catalytic applications in the last decade,[7, 49-53] owning to their enhanced selectivity caused by the dilute species (such as Pt, Ag, Pd, and Rh) and synergistic effects with the host (Au and Ag, among others). In recent work, the effect of pretreatment on the catalytic activity of dilute (4 to 8 at.% Pd in Au) BNPs for the

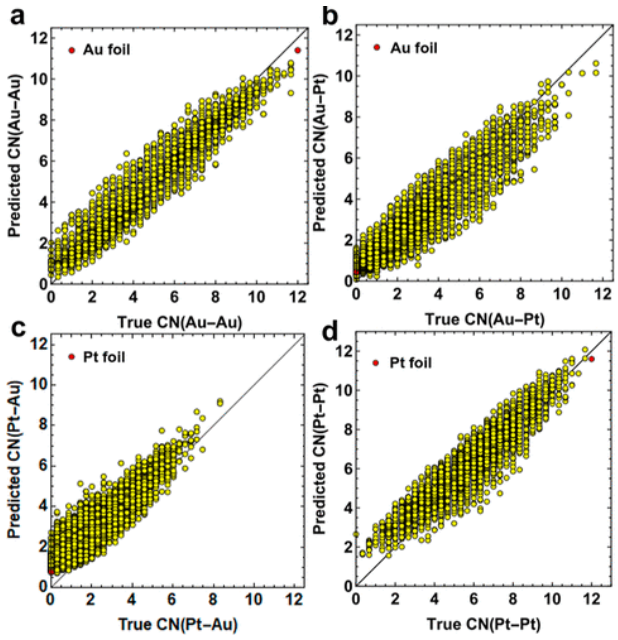

Fig 3. Validation of the NN using the predicted (a) CN_{Au-Au}, (b) CN_{Au-Pt}, (c) CN_{Pt-Au}, and (d) CN_{Pt-Pt} vs true values. Reproduced with permission from Ref. 40.

hydrogen-deuterium (HD) exchange reaction was investigated.[54] From a combination of catalytic activity measurements, ML-enabled spectroscopic analysis, and first-principles-based kinetic modelling, it was demonstrated that active species for HD exchange reaction are surface Pd ensembles containing only a few (from 1 to 3) Pd atoms.[23] The catalyst Pd K-edge absorption coefficient data in the XANES region (Fig. 4a) show the shifts toward, or away from, the reference Pd bulk spectrum of the data collected in the 8 at.% Pd-in-Au sample, depending on the treatments (S0-S4, described in Fig. 4). For example, after treatment of the initial sample with O_2 (S0 to S1), the center of mass of the absorption coefficient shifts to the positive energy direction (*i.e.*, toward the Pd reference), and, after treatment with hydrogen (S1 to S2 to S3), to the lower energies (*i.e.*, away from the bulk Pd and past S0 (Fig. 4a)). Those negative shifts are consistent with the increase in the number of Pd-Au neighbours resulting from Pd dissolution into the Au host, while the positive shift is associated with the segregation of Pd and ensemble formation (Pd_nAu).

Partial CNs ($\boldsymbol{C_{Pd-Pd}}$ and $\boldsymbol{C_{Pd-Au}}$) were obtained using the NN-XANES method (Fig. 4b). The trends shown in Fig. 4b are consistent with the qualitative observation (*vide supra*) made on the basis of Fig. 4a. This end, the Pd-Pd CNs slightly increase, and the Pd-Au CNs decrease after the initial treatment in O_2 (from S0 to S1), followed by the decrease of Pd-Pd CNs (and increase of Pd-Au) after subsequent H_2 treatments (from S1 to S2 to S3). In that work, the comparison of EXAFS analysis and NN-XANES analysis results was shown to favour the latter due to the poor sensitivity of EXAFS to the nearest neighbour CNs of the dilute element (*e.g.*, Pd-Pd vis. Pd-Au). In contrast, the NN-XANES method worked better because the neural network has a "good eye" on various features required for the CN prediction. This is an improvement compared to the standard, least squares fitting method used in EXAFS data analysis that relies on a sole criterion: minimization of the mean squared error.

2.3 Machine learning-assisted EXAFS Analysis

If the previous section made an impression on the reader that NN-XANES is a universal panacea for all challenges in XAFS experiment and data analysis, this was not our intention. In cases when EXAFS data in BNPs is of good quality, they contain a treasure trove of information about the structure and dynamics of nearest neighbouring atoms with respect to the X-ray absorbing atoms, well

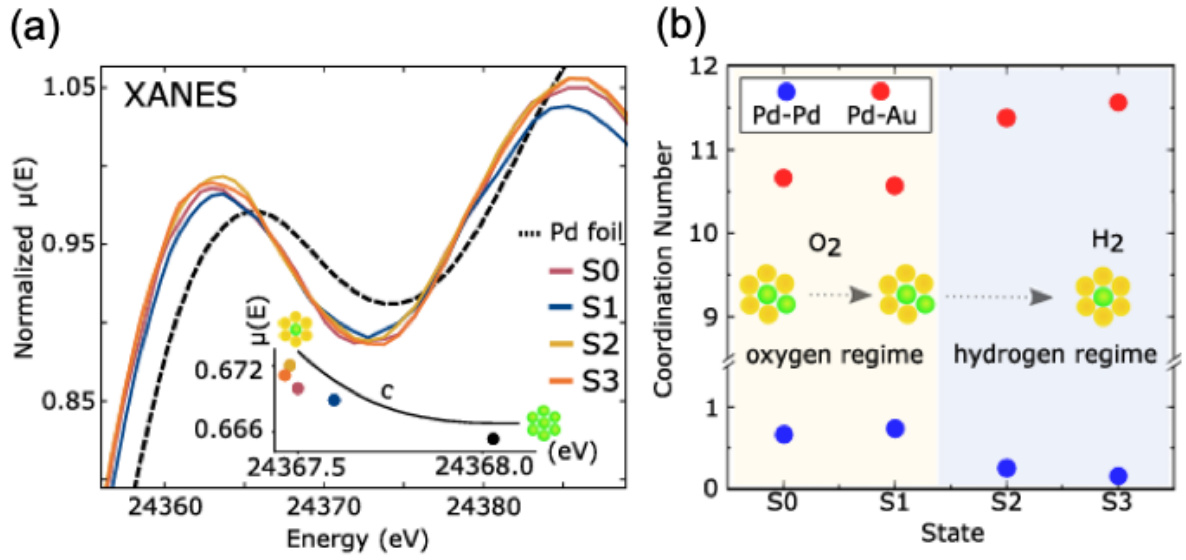

Fig. 4. Normalized XANES (a) collected for the different samples of dilute (8 at.% Pd in Au) BNPs after different pretreatments, shown as "O_2 regime" and "H_2 regime" in color bands (b). The inset of (a) shows a shift in the spectral center of mass "c". CNs from NN-XANES are consistent with Pd atoms having more Pd neighbors after O_2 treatment and less Pd neighbors after H_2 treatment. Atomic Pd ensembles in (a) and (b) are depicted with bird's-eye-view schematics (yellow = Au; green=Pd). Reproduced with permission from Ref. 23.

beyond a limited amount of information encoded in XANES. While the information content in XANES is a separate topic, and the ML methods that probe it by using the latent space dimension of the autoencoders have emerged only recently,[55] the methods for establishing the information content in EXAFS, such as that relying on the Nyquist criterion, have been in use for half a century.[56] For example, while NN-XANES can determine ca. four parameters from Pt L_3-edge data in a nanoparticle (such as the first four CNs),[38] EXAFS spectra (for the same type of nanoparticle sample) that has *k*-range from 2 to 20 Å^{-1} and the fitting range in r-space from 2 to 6.2 Å,[57] has $\sim 2 \cdot 18 \cdot 5.2/\pi \approx 60$ relevant independent data points. That means up to 59 fitting variables can, in principle, be used to fit these data and describe the local environment up to the fifth coordination shell (*i.e.*, much more information than encoded in the XANES spectrum).

Just as it was shown for the monometallic particles, the correct interpretation of EXAFS data in BNPs relies strongly on the validity of the key assumption. This assumption is that a (unknown) radial distribution function (RDF) of neighbours around the X-ray absorbing atoms is quasi-Gaussian; that is, a small number of terms in the cumulant expansion suffices to reproduce experimental EXAFS theoretically.[58] When the disorder is strongly asymmetric (as is the case in ultrasmall NPs with strong surface-, ligand-, and/or substrate-induced asymmetry[59-62]), the standard approach breaks down due to the inability of the fitting method to extract a large number of cumulant terms, whereas an alternative approach, based on the use of supervised ML, can be efficiently used instead. In that method, initially demonstrated for resolving the RDF in disordered, intermediate structures formed during the phase transition of Fe from bcc to fcc phases,[63] the theoretical EXAFS equation is expressed in terms of the unknown, $g(r) = dN/dr$, defined as the number of neighbors, dN, in the thin shell (with thickness dr) at distance r around the absorber. For bimetallic alloys (A_xB_y), the equation expresses EXAFS of the A-B single scattering path as follows:[64]

$$\chi_{AB}(k) = S_{0,A}^2 \int_0^{+\infty} F_{AB}(k,R) g_{AB}(R) \sin(2kR + \phi_{AB}(k,R)) \frac{dR}{kR^2}. \quad (4)$$

Here, $F_{AB}(k,R)$ and $\phi_{AB}(k,R)$ are scattering amplitude and phase functions that can be calculated theoretically, and $S_{0,A}^2$ is the amplitude reduction factor. Therefore, by using a theoretical training set constructed using Eq. (4), the unknown distributions ($g_{AB}(R), g_{AA}(R), g_{BB}(R), g_{BA}(R)$) can be predicted on the experimental EXAFS data directly, without *a priori* assumption about their functional form. After that, the CNs and interatomic distances for different types of neighbouring pairs (*e.g.*, A-B) can be calculated by integrating the corresponding RDF over the range of the corresponding coordination shell (*i.e.*, between the $(i-1)$-th and i-th minima of the $g_{AB}(R)$):

$$C_{i,AB} = \int_{R_{i-1,AB}}^{R_{i,AB}} g_{AB}(R)\, dR,$$

$$\langle R \rangle_{i,AB} = \frac{1}{C_{i,AB}} \int_{R_{i-1,AB}}^{R_{i,AB}} g_{AB}(R) R\, dR. \quad (5)$$

Because inversion of Eq. (4) is an ill-posed problem, it is important to validate the resultant distributions using the "ground truth", such as comparing them with distributions generated using molecular dynamics simulations. More discussion about the benefits of "objective" neural network training for RDF determination is given in the end of this Section.

2.4 Examples of the use of ML-EXAFS approach for structural characterization of BNP catalysts

The first work showing the application of the NN-EXAFS method to the analysis of BNPs was applied to Pd-Au particles.[64] The resultant CNs and interatomic distances are shown in Figs. 5A-D and E-F, respectively. As shown in Fig. 5F, the concentration dependencies for the Pd-Pd and Au-Au distances are almost the same for the 2nd coordination shell, but the Pd-Au pairs have unexpectedly short lengths, hinting at the segregation of Pd to the BNP surface at low Pd concentration. This conclusion would have been impossible to obtain by conventional EXAFS analysis. [64]

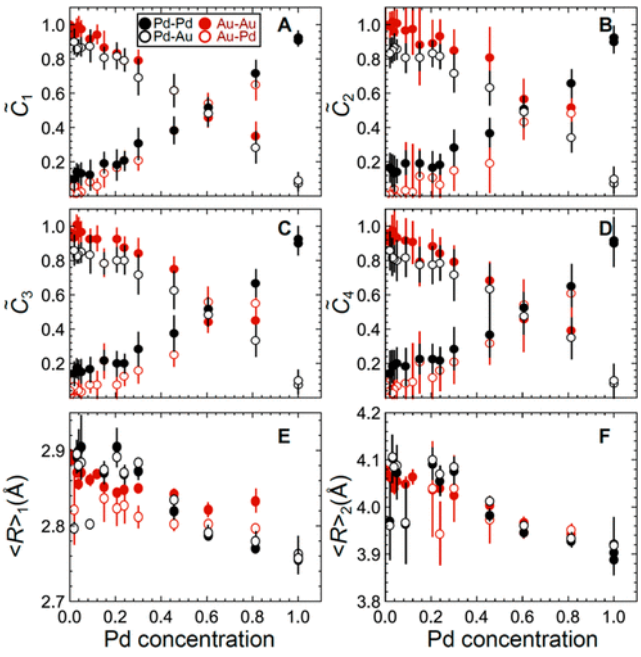

Fig. 5. Concentration dependencies of the normalized CNs Č1, Č2, Č3, and Č4 for the first four coordination shells (A–D) and average interatomic distances R for the first two coordination shells (E, F) obtained by integration of PRDFs, extracted by NN from experimental EXAFS data. Reproduced with permission from Ref. 56.

Another example of the use of the NN-EXAFS method is the study of Cu-Zn nano-catalysts, utilized for electrochemical reduction of CO_2. As discussed above, it is challenging to understand the evolution of bimetallic structures under reaction conditions, especially with low Z-contrast, which is the case for Cu and Zn. The NN-EXAFS approach was applied in this work for Zn and Cu K-edge EXAFS. It was generalized to account for the oxidized and partially oxidized Cu-Zn catalysts for CO_2 reduction reaction (CO_2RR).[65] Partial Cu–O and Cu–M (M = Cu, Zn) RDFs were extracted from Cu K-edge EXAFS data for as-prepared samples and samples in their final state under CO_2RR conditions, as shown in Fig. 6 (a, b).[65] The position of the maximum of the 3rd Cu–M RDF peak (located at ca. 4.5 Å) for Cu_{100}, $Cu_{70}Zn_{30}$, $Cu_{50}Zn_{50}$, and $Cu_{30}Zn_{70}$ NP samples corresponds to the interatomic distance in the 3rd coordination shell in the metallic phase. Partial Zn–O and Zn–M (M = Zn, Cu) RDFs were extracted from

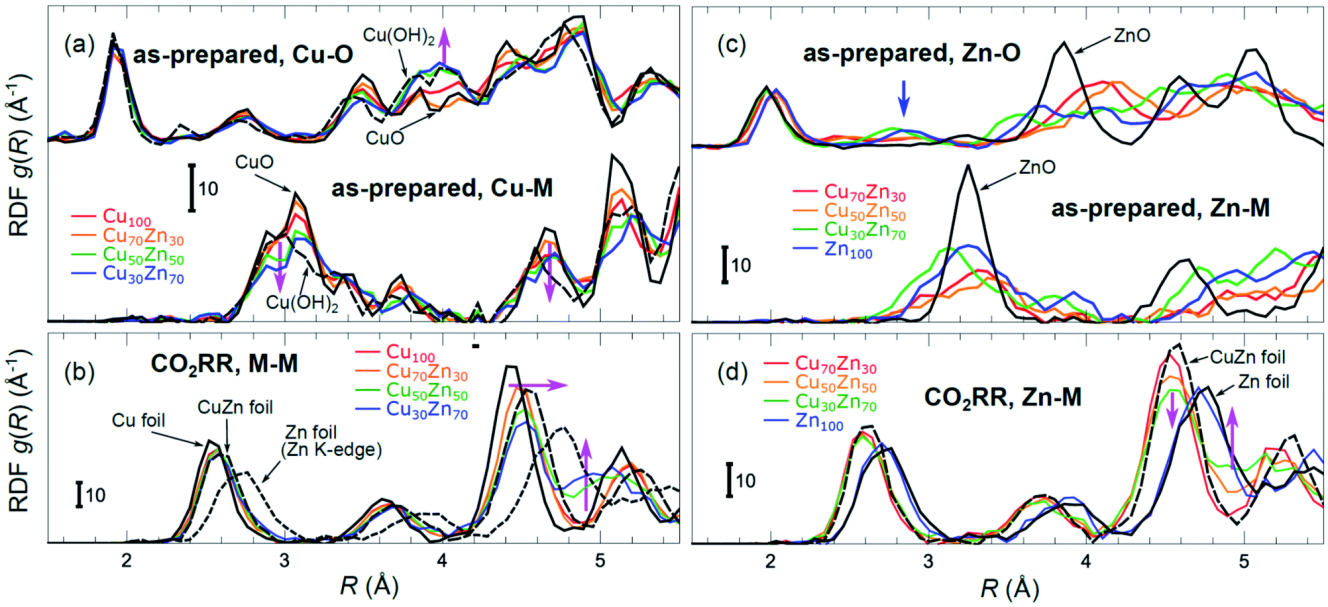

Fig. 6. Cu–O and Cu–M (M = Cu or Zn) RDFs extracted by NN from experimental Cu K-edge EXAFS for Cu_{100}, $Cu_{70}Zn_{30}$, $Cu_{50}Zn_{50}$, and $Cu_{30}Zn_{70}$ BNPs in their as-prepared state (a) as well as in their final state after 1–7 hr under CO_2RR conditions (b). Zn–O and Zn–M RDFs extracted by NN from experimental Zn K-edge EXAFS data for $Cu_{70}Zn_{30}$, $Cu_{50}Zn_{50}$, $Cu_{30}Zn_{70}$, and Zn_{100} BNPs in their as-prepared state (c) as well as in their final state after 1–7 h under CO_2RR conditions (d). Data extracted from Cu K-edge EXAFS for reference compounds (Cu foil, CuZn brass foil, CuO, and $Cu(OH)_2$), as well as Zn–Zn RDF, extracted from Zn K-edge EXAFS for a Zn foil are also shown for comparison in (a) and (b). Zn–O and Zn–Zn RDFs extracted by the NN from experimental Zn K-edge EXAFS for reference compounds (Zn foil, CuZn brass foil, and ZnO) are shown in (c) and (d). RDFs are shifted vertically for clarity. Reproduced with permission from Ref. 57.

Zn K-edge EXAFS data for the BNP samples in their as-prepared state as well as in their final state under CO_2RR conditions, as shown in Fig. 6 (c, d).[65] Time-dependent EXAFS data from both Cu and Zn K-edge were analysed by NN-EXAFS to monitor the structural transformation of CuZn nanoparticles in real time under CO_2RR conditions. NN-EXAFS analysis revealed a gradual Cu-Zn alloying process and a transition from a close-packed to a more disordered structure.[65]

In summary of this section, we mention that in the original NN-EXAFS method, the neural network training was performed using molecular dynamics simulations. MD-EXAFS was used to account for the dynamic, temperature-dependent disorder, contributing to the RDF and, therefore, to EXAFS spectra.[63, 64] Recently, an "objective" method for NN training (dubbed "ONNE"), that does not rely on molecular dynamics simulations, was proposed and used for training the NN and "inverting" EXAFS spectra in transition metal and actinide complexes in molten salts.[66, 67]

3. Outlook

If the development of advanced ML methods for analysing XAFS data in BNPs continues to progress, we anticipate the emergence of new and enhanced capabilities. Among them, there is a long-standing problem of heterogeneous distribution of metal species that absorb X-rays, ranging from the coexistence of different oxidation states to broad distributions of nanoparticle sizes and shapes and their compositional motifs. Several articles reported analyses of such distributions and their artifacts on EXAFS spectra in BNPs,[48, 68, 69] and developed strategies to account for the details of the distribution, either using a combination of EXAFS and electron microscopy, as one example,[44-46, 70] or methods adopted in chemometrics, such as principal component analysis (PCA) and multivariate curve resolution - alternating least squares (MCR-ALS) for XANES studies, as another.[43] Due to their unique spectral signatures, XANES regions of the X-ray absorbing elements coexisting in the sample containing a broad distribution of BNPs can be, in principle, also deconvoluted and separated using PCA and MCR-ALS, similar to what was done for Pd K-edge in Pd-Cu size selective clusters.[43] A network classifier would take the deconvoluted spectra and attribute them to a specific class, specific to, for example, the oxidation state of the same element, followed by separate structural refinement of each deconvoluted spectra using either conventional EXAFS fitting or NN-XANES/NN-EXAFS methods.

Other opportunities are foreseeable for new materials proposed for stable and selective catalysts based on high entropy alloys (HEA) and oxides.[71] Due to the similarity of constituting elements in the HEAs, their conventional EXAFS analysis is severely limited by the poor spectral content of different atomic species.[72] This is quite similar to what was, for a long time, a limitation on EXAFS analysis of bimetallic alloys containing neighbouring elements.[47] The chief challenge is to discriminate between the contributions to XAFS of A-A, A-B (A-C, A-D, etc.) in the alloy where A, B, C, D, etc. are the elements with poor Z contrast. With the aid of NN-XANES, such a task can be solved (in principle) because of the excellent sensitivity of the neural network to the spectral features due to the bonding of atoms of different types, as demonstrated recently.[44-46] For L absorption edges, these features were shown to be associated with the white line intensities that redistribute between different alloying elements

compared to their pure metal edge intensities due to the electron charge transfer between different atomic species.[73] The capability of NN-XANES for spectral recognition will be further elevated when the data with high energy resolution fluorescence detection (HERFD) are used, whereas the features in the main peak region of the absorption coefficient in BNPs are enhanced[74-81] due to lower spectral broadening. There are also exciting opportunities to increase the spatial resolution of local structural probes by relying on the small (a few nm) spot size in scanning transmission electron microscopy – electron energy loss spectroscopy (STEM-EELS) applications. Electron energy loss – near edge structure (ELNES) has similar information to XANES and can be, in principle, mapped on the structural and electronic descriptors[82] to the local environment of the resonant atom, albeit with 1000 times better spatial resolution than the most currently used X-ray probes.

As the complexity of nanoparticles increases to include five or more different elemental components, self-segregation of different atoms within the particles, changes to the particle size and shape, etc., more advanced spectroscopic characterization methods are required. Atomically-resolved understanding of this structure is of the utmost priority to understand the function of the material, especially for catalysis that requires precise atomic arrangements at the nanoparticle surface. Advances in ML and NN-XANES open the door to identifying these key structural factors that have remained challenging to impossible to achieve with conventional characterization methods.

Conflicts of interest

There are no conflicts to declare.

Acknowledgements

The work primarily supported by the National Science Foundation under grants 2203858 (to A.I.F.) and 2203862 (to M.R.K.).

References

1. V. Dupuis, G. Khadra, A. Hillion, A. Tamion, J. Tuaillon-Combes, L. Bardotti and F. Tournus, *Physical Chemistry Chemical Physics*, 2015, **17**, 27996-28004.
2. I. Wachs, A. Chakrabarti, M. H. Zhu, S. Lwin, C. Keturakis and Y. D. Tang, *Abstr Pap Am Chem S*, 2015, **250**, 1115.
3. D. A. Garfinkel, G. Pakeltis, N. Tang, I. N. Ivanov, J. D. Fowlkes, D. A. Gilbert and P. D. Rack, *ACS Omega*, 2020, **5**, 19285-19292.
4. S. S. Mohammed Ameen and K. M. Omer, *ACS Applied Materials & Interfaces*, 2024, **16**, 31895-31921.
5. L. Chen, H.-F. Wang, C. Li and Q. Xu, *Chemical Science*, 2020, **11**, 5369-5403.
6. J. Wang, S. Chen, P. Ticali, P. Summa, S. Mai, K. Skorupska and M. Behrens, *Nanoscale*, 2024, **16**, 17378-17392.
7. J. D. Lee, J. B. Miller, A. V. Shneidman, L. Sun, J. F. Weaver, J. Aizenberg, J. Biener, J. A. Boscoboinik, A. C. Foucher, A. I. Frenkel, J. E. S. van der Hoeven, B. Kozinsky, N. Marcella, M. M. Montemore, H. T. Ngan, C. R. O'Connor, C. J. Owen, D. J. Stacchiola, E. A. Stach, R. J. Madix, P. Sautet and C. M. Friend, *Chemical Reviews*, 2022, **122**, 8758-8808.
8. W. Yu, M. D. Porosoff and J. G. Chen, *Chemical Reviews*, 2012, **112**, 5780-5817.
9. C. Especel, G. Lafaye and F. Epron, *ChemCatChem*, 2023, **15**, e202201478.
10. F. Gao and D. W. Goodman, *Chemical Society Reviews*, 2012, **41**, 8009-8020.
11. K.-H. Huynh, X.-H. Pham, J. Kim, S. H. Lee, H. Chang, W.-Y. Rho and B.-H. Jun, *Journal*, 2020, **21**.
12. G. Sharma, A. Kumar, S. Sharma, M. Naushad, R. Prakash Dwivedi, Z. A. Alothman and G. T. Mola, *Journal of King Saud University - Science*, 2019, **31**, 257-269.
13. A. H. Hatta, A. A. Jalil, N. S. Hassan, M. Y. S. Hamid, A. F. A. Rahman, L. P. Teh and D. Prasetyoko, *International Journal of Hydrogen Energy*, 2022, **47**, 30981-31002.
14. L. Liu and A. Corma, *Chem Rev*, 2023, **123**, 4855-4933.
15. K. Zhao, Y. Shu, F. Li and G. Peng, *Green Energy & Environment*, 2023, **8**, 1043-1070.
16. S. Hu, F. Che, B. Khorasani, M. Jeon, C. W. Yoon, J.-S. McEwen, L. Scudiero and S. Ha, *Applied Catalysis B: Environmental*, 2019, **254**, 685-692.
17. K. D. Gilroy, A. Ruditskiy, H.-C. Peng, D. Qin and Y. Xia, *Chemical Reviews*, 2016, **116**, 10414-10472.
18. F. Tao and M. Salmeron, *Science*, 2024, **386**, eadq0102.
19. D. C. Koningsberger and R. Prins, *X-ray absorption: principles, applications, techniques of EXAFS, SEXAFS and XANES*, 1987.
20. J. H. Sinfelt, *ACCOUNTS of chemical research*, 1987, **20**, 134-139.
21. J. H. Sinfelt, G. H. Via and F. W. Lytle, *The Journal of Chemical Physics*, 1982, **76**, 2779-2789.
22. S. Xie, S.-I. Choi, X. Xia and Y. Xia, *Current Opinion in Chemical Engineering*, 2013, **2**, 142-150.
23. N. Marcella, J. S. Lim, A. M. Płonka, G. Yan, C. J. Owen, J. E. S. van der Hoeven, A. C. Foucher, H. T. Ngan, S. B. Torrisi, N. S. Marinkovic, E. A. Stach, J. F. Weaver, J. Aizenberg, P. Sautet, B. Kozinsky and A. I. Frenkel, *Nature Communications*, 2022, **13**, 832.
24. M. Luneau, T. Shirman, A. Filie, J. Timoshenko, W. Chen, A. Trimpalis, M. Flytzani-Stephanopoulos, E. Kaxiras, A. I. Frenkel, J. Aizenberg, C. M. Friend and R. J. Madix, *Chemistry of Materials*, 2019, **31**, 5759-5768.
25. M. Luneau, E. Guan, W. Chen, A. C. Foucher, N. Marcella, T. Shirman, D. M. A. Verbart, J. Aizenberg, M. Aizenberg, E. A. Stach, R. J. Madix, A. I. Frenkel and C. M. Friend, *Communications Chemistry*, 2020, **3**, 46.
26. M. Luneau, T. Shirman, A. C. Foucher, K. Duanmu, D. M. A. Verbart, P. Sautet, E. A. Stach, J. Aizenberg, R. J. Madix and C. M. Friend, *ACS Catalysis*, 2020, **10**, 441-450.
27. D. Liu, Y. Li, M. Kottwitz, B. Yan, S. Yao, A. Gamalski, D. Grolimund, O. V. Safonova, M. Nachtegaal, J. G. Chen, E. A. Stach, R. G. Nuzzo and A. I. Frenkel, *Acs Catal*, 2018, **8**, 4120-4131.
28. A. C. Foucher, S. Yang, D. J. Rosen, R. Huang, J. B. Pyo, O. Kwon, C. J. Owen, D. F. Sanchez, I. I. Sadykov, D. Grolimund, B. Kozinsky, A. I. Frenkel, R. J. Gorte, C. B. Murray and E. A. Stach, *Journal of the American Chemical Society*, 2023, **145**, 5410-5421.
29. A. C. Foucher, N. Marcella, J. D. Lee, R. Tappero, C. B. Murray, A. I. Frenkel and E. A. Stach, *The Journal of Physical Chemistry C*, 2022, **126**, 1991-2002.
30. A. C. Foucher, N. Marcella, J. D. Lee, D. J. Rosen, R. Tappero, C. B. Murray, A. I. Frenkel and E. A. Stach, *ACS Nano*, 2021, **15**, 20619-20632.
31. P. K. Routh, E. Redekop, S. Prodinger, J. E. S. van der Hoeven, K. R. G. Lim, J. Aizenberg, M. Nachtegaal, A. H. Clark and A. I. Frenkel, *Nature Communications*, 2024, **15**, 6736.

32. D. Ferri, M. S. Kumar, R. Wirz, A. Eyssler, O. Korsak, P. Hug, A. Weidenkaff and M. A. Newton, *Phys Chem Chem Phys*, 2010, **12**, 5634-5646.
33. G. L. Chiarello and D. Ferri, *Phys Chem Chem Phys*, 2015, **17**, 10579-10591.
34. C. F. J. König, J. A. van Bokhoven, T. J. Schildhauer and M. Nachtegaal, *The Journal of Physical Chemistry C*, 2012, **116**, 19857-19866.
35. J. J. Rehr and R. C. Albers, *Reviews of Modern Physics*, 2000, **72**, 621-654.
36. Y. Joly, *Phys Rev B*, 2001, **63**, 125120.
37. J. Timoshenko and A. I. Frenkel, *ACS Catalysis*, 2019, **9**, 10192-10211.
38. J. Timoshenko, D. Lu, Y. Lin and A. I. Frenkel, *The Journal of Physical Chemistry Letters*, 2017, **8**, 5091-5098.
39. N. Marcella, Y. Liu, J. Timoshenko, E. Guan, M. Luneau, T. Shirman, A. M. Plonka, J. E. S. van der Hoeven, J. Aizenberg, C. M. Friend and A. I. Frenkel, *Physical Chemistry Chemical Physics*, 2020, **22**, 18902-18910.
40. S. B. Torrisi, M. R. Carbone, B. A. Rohr, J. H. Montoya, Y. Ha, J. Yano, S. K. Suram and L. Hung, *npj Computational Materials*, 2020, **6**, 109.
41. A. Ghose, M. Segal, F. Meng, Z. Liang, M. S. Hybertsen, X. Qu, E. Stavitski, S. Yoo, D. Lu and M. R. Carbone, *Physical Review Research*, 2023, **5**, 013180.
42. M. R. Carbone, S. Yoo, M. Topsakal and D. Lu, *Physical Review Materials*, 2019, **3**, 033604.
43. Y. Liu, A. Halder, S. Seifert, N. Marcella, S. Vajda and A. I. Frenkel, *ACS Applied Materials & Interfaces*, 2021, **13**, 53363-53374.
44. Y. Liu, M. Xie, N. Marcella, A. C. Foucher, E. A. Stach, M. R. Knecht and A. I. Frenkel, *ACS Applied Nano Materials*, 2022, **5**, 8775-8782.
45. M. Xie, R. Shimogawa, Y. Liu, L. Zhang, A. C. Foucher, P. K. Routh, E. A. Stach, A. I. Frenkel and M. R. Knecht, *ACS Nano*, 2024, **18**, 3286-3294.
46. M. Xie, R. Shimogawa, Y. Liu, L. Zhang, A. C. Foucher, P. K. Routh, E. A. Stach, A. I. Frenkel and M. R. Knecht, *ACS Nano*, 2024, **18**, 24604-24604.
47. L. D. Menard, Q. Wang, J. H. Kang, A. J. Sealey, G. S. Girolami, X. Teng, A. I. Frenkel and R. G. Nuzzo, *Physical Review B*, 2009, **80**, 064111.
48. A. I. Frenkel, *Chemical Society Reviews*, 2012, **41**, 8163-8178.
49. A. P. Minne, T. Maxson, T. Szilvási and J. W. Harris, *Catalysis Science & Technology*, 2024, **14**, 1534-1549.
50. M. M. Montemore, R. J. Madix and E. Kaxiras, *The Journal of Physical Chemistry C*, 2016, **120**, 16636-16640.
51. L. V. Moskaleva, S. Röhe, A. Wittstock, V. Zielasek, T. Klüner, K. M. Neyman and M. Bäumer, *Physical Chemistry Chemical Physics*, 2011, **13**, 4529-4539.
52. W.-Y. Yu, L. Zhang, G. M. Mullen, G. Henkelman and C. B. Mullins, *The Journal of Physical Chemistry C*, 2015, **119**, 11754-11762.
53. A. P. Minne, E. P. Iaia, E. Stavitski and J. W. Harris, *ACS Catalysis*, 2024, **14**, 17209-17225.
54. J. E. S. van der Hoeven, H. T. Ngan, A. Taylor, N. M. Eagan, J. Aizenberg, P. Sautet, R. J. Madix and C. M. Friend, *ACS Catalysis*, 2021, **11**, 6971-6981.
55. P. K. Routh, Y. Liu, N. Marcella, B. Kozinsky and A. I. Frenkel, *The Journal of Physical Chemistry Letters*, 2021, **12**, 2086-2094.
56. E. A. Stern, *Physical Review B*, 1993, **48**, 9825-9827.
57. A. I. Frenkel, C. W. Hills and R. G. Nuzzo, *The Journal of Physical Chemistry B*, 2001, **105**, 12689-12703.
58. A. I. Frenkel, V. S. Machavariani, A. Rubshtein, Y. Rosenberg, A. Voronel and E. A. Stern, *Physical Review B*, 2000, **62**, 9364-9371.
59. B. S. Clausen, H. Topsøe, L. B. Hansen, P. Stoltze and J. K. Nørskov, *Japanese Journal of Applied Physics*, 1993, **32**, 95.
60. A. Yevick and A. I. Frenkel, *Physical Review B*, 2010, **81**, 115451.
61. S. T. Chill, R. M. Anderson, D. F. Yancey, A. I. Frenkel, R. M. Crooks and G. Henkelman, *ACS Nano*, 2015, **9**, 4036-4042.
62. J. Timoshenko and A. I. Frenkel, *Catalysis Today*, 2017, **280**, 274-282.
63. J. Timoshenko, A. Anspoks, A. Cintins, A. Kuzmin, J. Purans and A. I. Frenkel, *Physical Review Letters*, 2018, **120**, 225502.
64. J. Timoshenko, C. J. Wrasman, M. Luneau, T. Shirman, M. Cargnello, S. R. Bare, J. Aizenberg, C. M. Friend and A. I. Frenkel, *Nano Letters*, 2019, **19**, 520-529.
65. J. Timoshenko, H. S. Jeon, I. Sinev, F. T. Haase, A. Herzog and B. Roldan Cuenya, *Chemical Science*, 2020, **11**, 3727-3736.
66. N. Marcella, S. Lam, V. S. Bryantsev, S. Roy and A. I. Frenkel, *Physical Review B*, 2024, **109**, 104201.
67. K. Zheng, N. Marcella, A. L. Smith and A. I. Frenkel, *The Journal of Physical Chemistry C*, 2024, **128**, 7635-7642.
68. A. I. Frenkel, Q. Wang, S. I. Sanchez, M. W. Small and R. G. Nuzzo, *The Journal of Chemical Physics*, 2013, **138**.
69. A. I. Frenkel, A. Yevick, C. Cooper and R. Vasic, *Annual Review of Analytical Chemistry*, 2011, **4**, 23-39.
70. Z. Duan, J. Timoshenko, P. Kunal, S. D. House, H. Wan, K. Jarvis, C. Bonifacio, J. C. Yang, R. M. Crooks, A. I. Frenkel, S. M. Humphrey and G. Henkelman, *Nanoscale*, 2018, **10**, 22520-22532.
71. D. Sur, E. F. Holcombe, W. H. Blades, E. A. Anber, D. L. Foley, B. L. DeCost, J. Liu, J. Hattrick-Simpers, K. Sieradzki, H. Joress, J. R. Scully and M. L. Taheri, *High Entropy Alloys & Materials*, 2023, **1**, 336-353.
72. H. Joress, B. Ravel, E. Anber, J. Hollenbach, D. Sur, J. Hattrick-Simpers, M. L. Taheri and B. DeCost, *Matter*, 2023, **6**, 3763-3781.
73. W. Du, D. Su, Q. Wang, A. I. Frenkel and X. Teng, *Crystal Growth & Design*, 2011, **11**, 594-599.
74. J. Chen, Y. Z. Finfrock, Z. Wang and T.-K. Sham, *The Journal of Physical Chemistry C*, 2021, **125**, 2327-2333.
75. D. Friebel, D. J. Miller, D. Nordlund, H. Ogasawara and A. Nilsson, *Angewandte Chemie International Edition*, 2011, **50**, 10190-10192.
76. M. Filez, E. A. Redekop, J. Dendooven, R. K. Ramachandran, E. Solano, U. Olsbye, B. M. Weckhuysen, V. V. Galvita, H. Poelman, C. Detavernier and G. B. Marin, *Angewandte Chemie International Edition*, 2019, **58**, 13220-13230.
77. L. L. Van Loon, Y. Z. Finfrock, D. M. Meira, R. W. Burgess, G. Bevan and N. R. Banerjee, *Journal of Analytical Atomic Spectrometry*, 2025, **40**, 137-145.
78. A. Beheshti Askari, M. al Samarai, N. Hiraoka, H. Ishii, L. Tillmann, M. Muhler and S. DeBeer, *Nanoscale*, 2020, **12**, 15185-15192.
79. J. Wang, C.-S. Hsu, T.-S. Wu, T.-S. Chan, N.-T. Suen, J.-F. Lee and H. M. Chen, *Nature Communications*, 2023, **14**, 6576.
80. T. Penfold, L. Watson, C. Middleton, T. David, S. Verma, T. Pope, J. Kaczmarek and C. Rankine, *Machine Learning: Science and Technology*, 2024, **5**, 021001.
81. A. Martini, J. Timoshenko, P. Grosse, C. Rettenmaier, D. Hursán, G. Deplano, H. S. Jeon, A. Bergmann and B. Roldan Cuenya, *Physical Review Letters*, 2024, **133**, 228001.
82. S. P. Gleason, D. Lu and J. Ciston, *npj Computational Materials*, 2024, **10**, 221.